

Crystal growth and characterisation of $(\text{Dy}_x\text{La}_{1-x})_2\text{Ti}_2\text{O}_7$ crystals

R. Jacko¹, M. Mihalik^{2*}, M. Mihalik jr.², M. Zentková², P. Roupčová^{3,4}

¹USSE Research & Development, U. S. Steel Košice s.r.o., Slovak Republic

²Institute of Experimental Physics, Slovak Academy of Sciences, Watsonova 47, Košice, Slovak Republic

³Institute of Physics of Materials, ASCR, v. v. i., Brno, Czech Republic

⁴Brno University of Technology, Central European Institute of Technology, Brno, Czech Republic

Received 3 September 2019, received in revised form 12 November 2019, accepted 11 December 2019

Abstract

$\text{LaTiO}_{3.5}$ crystals were grown by optical floating zone technique in air, O_2 , or Ar. Crystal structure varies between orthorhombic $Pna2_1$ (air, O_2) and monoclinic $P2_1$ (Ar). Crystals are transparent (air, O_2) or opaque (Ar) with amber or black colour. Magnetisation resembles the properties of $\text{LaTiO}_{3.5}$. $(\text{Dy}_x\text{La}_{1-x})_2\text{Ti}_2\text{O}_7$ crystals were grown in O_2 . The solubility of dopant (La or Dy) in the parent compound is limited. Two phases with $Pna2_1$ and $Fd\bar{3}m$ structure coexist in the range from $x = 0.32$ to 0.68 . The a -axis of $Pna2_1$ is intact by substitution of La^{3+} by Dy^{3+} ; both b - and c -axes decrease. The a -axis of $Fd\bar{3}m$ increases with substitution of Dy^{3+} by La^{3+} and the spin freezing temperature T_f shifts to a higher temperature. Either of the new magnetic phase ($Pna2_1$ structure) or dynamical behaviour of spins in $Fd\bar{3}m$ phase exists below $x = 0.68$ in the range between the transition to ‘spin ice’ state T_i and T_f .

Key words: optical floating zone, single crystals, crystal structure, ferroelectrics, spin ice

1. Introduction

LaTiO_x compounds are structurally related to perovskites, and there are two known phases. The first, $x = 3.50$, is a 2D layered-type ferroelectric. The second, $x = 3.00$, is a weak ferromagnet with a 3D orthorhombic distorted perovskite structure. The physical properties of lanthanum titanium oxides strongly depend on the content of oxygen in the material [1, 2]. LaTiO_3 is an antiferromagnetic Mott insulator with a pseudo-cubic perovskite crystal structure of GdFeO_3 type (space group $Pbnm$) [3–5]. This structure arises from the ideal perovskite (space group $Pm\bar{3}m$) by tilting the TiO_6 octahedron around a $[110]_c$ axis (subscript c denotes the notation with respect to the cubic perovskite lattice), followed by a rotation around the c -axis (or $[001]_c$ axis) [5]. The Néel temperature varies between $T_N = 130$ and 146 K, depending on the exact oxygen stoichiometry [5–7]. Interestingly, a reduced total moment of about 0.45 – $0.57 \mu_B$ in the ordered state has been observed [5–7]. One could speculate that this suggests the presence of an orbital angular momentum that is antiparallel to the spin momen-

tum [7, 8]. Recently, however, Keimer et al. [9] observed that the orbital momentum must be quenched. To explain the reduced moment, they proposed the presence of strong orbital fluctuations in the system. This seems to be supported by the theoretical study of Khaliullin and Maekawa [10], who suggested that LaTiO_3 is in a completely novel state of matter – an orbital liquid state. $\text{La}_2\text{Ti}_2\text{O}_7$ is a well-known high-temperature, ferroelectric compound (the Curie temperature $T_C \approx 1500^\circ\text{C}$), which exhibits a strong piezoelectric and electro-optic effect, has a high dielectric constant with a low-temperature coefficient and a low dielectric loss at microwave frequency, also possesses good photocatalytic activity [11–14]. $\text{La}_2\text{Ti}_2\text{O}_7$ does not form the expected isometric pyrochlore structure-type, as is typical for many of the heavy rare earth and transition metal oxides, but rather forms a layered structure comprised of slabs of the ABO_3 perovskite structure [11], which is monoclinic, $P2_1$ at room temperature, the structure becomes orthorhombic, $Cmc2_1$ at 780°C , and at 1500°C , it transforms into the paraelectric $Cmcm$ phase. The room temperature crystal structure of $\text{La}_2\text{Ti}_2\text{O}_7$ can be described in

*Corresponding author: e-mail address: mihalik@saske.sk

some cases by the $Pna2_1$ orthorhombic crystal structure [15]. On the other hand, $Dy_2Ti_2O_7$ is identified as a spin-ice material with the pyrochlore structure that crystallises into a face centred cubic structure $Fd\bar{3}m$ [16–20]. The dynamical freezing behaviour seen in $Dy_2Ti_2O_7$ differs from the critical slowing down observed in conventional disordered spin-glass materials. Another difference between the spin freezing in $Dy_2Ti_2O_7$ and that in conventional disordered spin glasses is the magnetic field dependence. Recently two ferroelectric transitions at $T_{C1} = 25$ K and $T_{C2} = 13$ K were observed in $Dy_2Ti_2O_7$ [17]. Remarkable magnetoelectric coupling was identified below the lower transition temperature, with significant suppression of the electric polarisation on an applied magnetic field.

In our paper, we focus on crystal growth, characterisation and magnetic properties of $(Dy_xLa_{1-x})_2Ti_2O_7$ system at low temperature, which may combine ferroelectric properties of $La_2Ti_2O_7$ with magnetic structure and ferroelectricity in $Dy_2Ti_2O_7$. In the first step, we studied the effect of crystal growth condition and oxygen content on the crystal structure of $LaTiO_x$ and in the second step, we investigated the change from pyrochlore crystal structure to orthorhombic distorted perovskite structure with substitution of La for Dy in $(Dy_xLa_{1-x})_2Ti_2O_7$ system.

2. Experimental details

$(Dy_xLa_{1-x})_2Ti_2O_7$ crystals were grown by the optical four mirror floating zone furnace model FZ-T-4000 (Crystal Systems INC). The grown crystals were characterised by scanning electron microscope (SEM) methods, including the energy-dispersive X-ray (EDX) microanalysis on the microscope TESCAN VEGA-3LMU equipped with EDX spectrometer BRUKER X-Flash 410M. SEM study confirmed the expected chemical composition and did not reveal any parasitic inclusions. The quality check and the alignment of the grown single crystals were performed by Real-time Laue Single Crystal Orientation Tool (Photon Science). The X-ray powder diffraction (XRPD) study was performed on powdered samples by the Rigaku Ultima IV diffractometer XRPD technique using $CuK_{\alpha 1, \alpha 2}$ doublet radiation and by the X'Pert (PanAnalytical) diffractometer using $Co K_{\alpha 1, \alpha 2}$ radiation with a help of qualitative analysis provided by HighScore[®] software and the JCPDS PDF-4 database [21]. For a quantitative analysis HighScore plus[®] with Rietveld structural models based on the ICSD database and Crystallography Open Database (COD) were applied. Powder data were treated using the Rietveld method implemented in FullProf software [22]. Prepared samples were also analysed by magnetisation and AC susceptibility measurements, which were

realised by MPMS SQUID magnetometer from Quantum Design.

3. Sample preparation and crystal growth

Floating zone technique with optical radiation heating was assigned to crystal growth of large single crystals of La-Ti-O, which crystallise as twinned (single) crystals with chemical formula $LaTiO_3$ and also $LaTiO_{3.5}$ ($La_2Ti_2O_7$) based on thermal treatment and preparation of starting material and type and condition of atmosphere used during crystal growth as type and pressure [23–26]. Starting materials for $LaTiO_x$ crystal growth can be different – the combination of $La_2O_3 + TiO_2 + TiO$ [1, 5], $La_2O_3 + TiO_2 + Ti$ [1], $Ti + TiO_2 + La$ [3], $La_2O_3 + Ti_2O_3$ or $La_2O_3 + TiO_2 + Ti_2O_3$ [23–26] materials can be used. The value of number x can be tuned mainly by proper combination of starting materials, and less effect is attributed to a simple reduction process by melting under the argon-hydrogen atmosphere (ratio 96:4) [1]. As was reported [23, 24], the best purity of final composition $LaTiO_3$ can be achieved by using La_2O_3 and Ti_2O_3 as starting materials, and we used this combination in our work, too. In this case, Ti^{3+} ion is present and we tried to prevent this oxidation number by preparation of starting materials and crystal growth under the Ar atmosphere and we studied the change of oxygen in the sample by manufacturing starting materials under air conditions and crystal growth process in air or oxygen. In all cases, we used a small overpressure of gas (about 0.1 MPa) and continuous gas flow.

Typical sample preparation of starting material we demonstrate for 15 g mass of $LaTiO_3$. We used high purity oxides of Ti_2O_3 (99.9 %, supplier: Sigma Aldrich, 4.6 g) and La_2O_3 (99.9 %, supplier: Sigma Aldrich, 10.4 g). The starting materials were mixed in a stoichiometric ratio in an agate mortar for at least 30 min to obtain a homogeneous powder. In the next step, the seed rod and feed rod were manufactured. The regular shape of both rods affects the stability of the melting zone, and that is why the preparation of feed rod is an essential and crucial part of crystal growth. The process of manual filling of a balloon with powder is time-consuming and tedious. During manual filling and pressing, geometrical imperfections and fluctuations in the density of pressed powder are usually introduced to feed or seed rods. Some of these imperfections can be eliminated by applying high isostatic pressure. For repeating crystal growth even with applying different growth conditions, feed rods should be the same (not only from the material side but also from the geometrical side). To minimise the geometric factor in the crystal growth process, we developed a device for the filling of balloons, which is shown in Fig. 1. We used latex one-end closed tubes (bal-

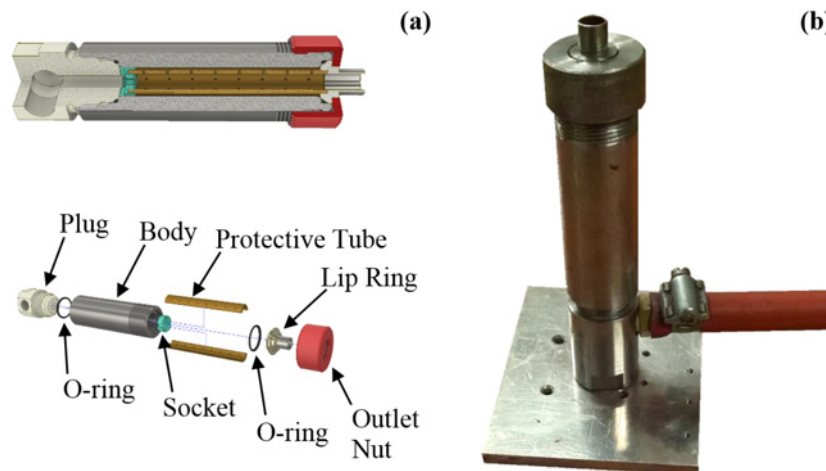


Fig. 1. Device for geometrically uniformed feed rod preparation; (a) a 3D visualisation, (b) the device.

loons) as containers for powder and the device shown in Fig. 1 to fill balloons with powder. Latex balloon is inserted to filler device by its closed end to split protective tube in suitable depth and loose end is pulled through a tube lip ring. The device is connected to a source of the vacuum by negative pressure inside of the device balloon which expands until it reaches the inner surface of the protective tube. Step by step small amount of the powder is added to the balloon and is subsequently compressed by a glass rod. This procedure is repeated many times to fill the balloon. In the next step isostatic pressure of above 200 MPa was used to produce rods with a hydraulic press into bars with a typical length of 6 to 7 cm (feed rod) and 3 cm (seed rod, both rods are shown in Fig. 2).

The balloons filled with powder were isostatically compressed into rods which were sintered in a vertical position in the air at a temperature $T = 1100^{\circ}\text{C}$ from 30 to 109 h in the commercial muffle furnace CMF1100 (MTI corporation). The scheme of a typical sintering temperature layout is shown in Fig. 2. Sintering in vertical position can reduce some geometrical faults of feed rod, for example, banana shape (bent rod). During the sintering of pressed rod in a vertical position, a small extension of rod occurred, which led to the generation of pores or even surface cracks. Sintering of rods under Ar atmosphere we realised at 1350°C in a horizontal position by GSL-1600 (MTI) furnace. Sintering procedure follows the solid-state reaction preparation route and the starting rods have already partially re-crystallised after heat treatment. Feed and seed rods surface become chalky after sintering (Fig. 2).

The width and length of the melting zone and condition on interface solid-liquid must be carefully watched, and only small correction of the lamp's power can be applied at this part of crystal growth. The porosity of the starting material affected the stability of the molten zone and the gas bubble appeared in

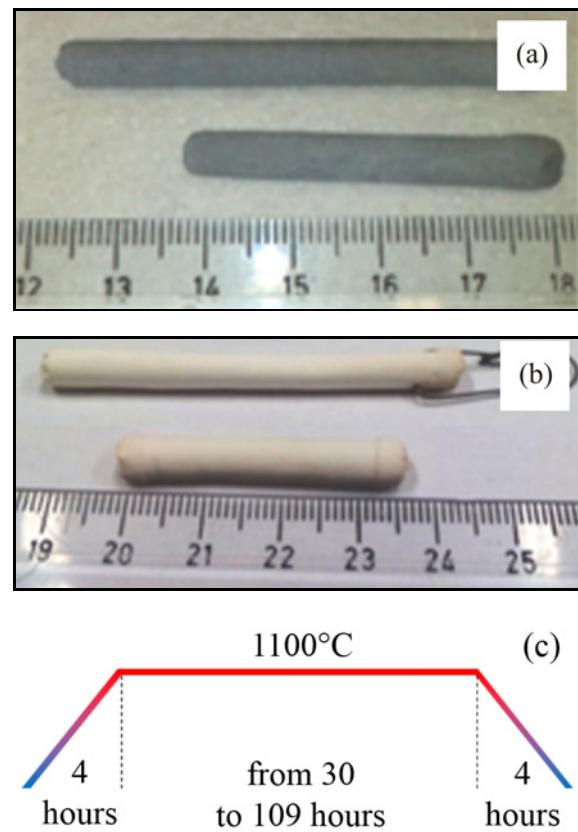


Fig. 2. Feed and seed rod (a) after isostatic compression, (b) after sintering, and (c) a scheme of temperature layout during sintering under air condition.

the melt zone. Small bubbles often merged and formed big bubbles, which were trapped in the melting zone and burst after some time and besides, the melt zone penetrated feed rod. On a series of screenshots taken during crystal growth in Fig. 3, the process of generating and merging bubbles is shown. Merging of bubbles is very dangerous for the stability of the melting

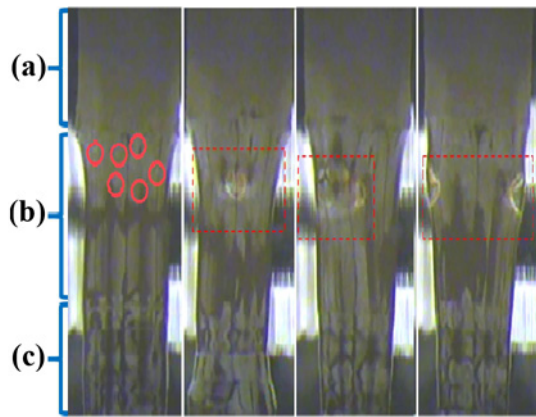


Fig. 3. Screenshots show the formation of large bubbles in the melting zone (red colour). In the background, we see the image of the hot wire of the halogen lamp (white), in the central part is seed rod ((a) – upper part), melting zone ((b) – middle), and grown crystal ((c) – bottom).

zone and in several cases resulted in the interruption of the crystal growth process. The crystals' growth speed was individually set up from 5 to 8 mm per hour. The

optimal crystal growth conditions for LaTiO_x crystals are pulling speed of about 6 mm per hour and counter-rotation of both seed and feed rods 15 rpm. A list of prepared crystals and conditions applied during crystal growth can be found in Table 1, and crystals photos are shown in Fig. 4. The colour of the crystals changes depending on the content of oxygen in the crystal from dark amber transparent colour for grown in O_2 , to light amber transparent colour for air and to opaque metallic shiny dark blue to black colour for Ar.

The Laue diffraction technique confirmed the single crystalline character of LaTiO_x . For example, the crystal No. 5 was grown as bi-crystal, separation (parting) surface is highlighted by a red arrow. Trial to orientate the crystal No. 5 was performed, which is shown in Fig. 5. Laue patterns from the lower part of a crystal No. 5 show relatively thin and sharp reflections. Those reflections are indicating the single crystalline character of the sample.

Single crystals of $\text{R}_2\text{Ti}_2\text{O}_7$ ($\text{R} = \text{Y, Gd, Tb, Dy, Ho, Er, Yb, and Lu}$) have been grown by the floating-zone technique in an image furnace [27–30] or by Czochralski method in iridium crucible with radio fre-

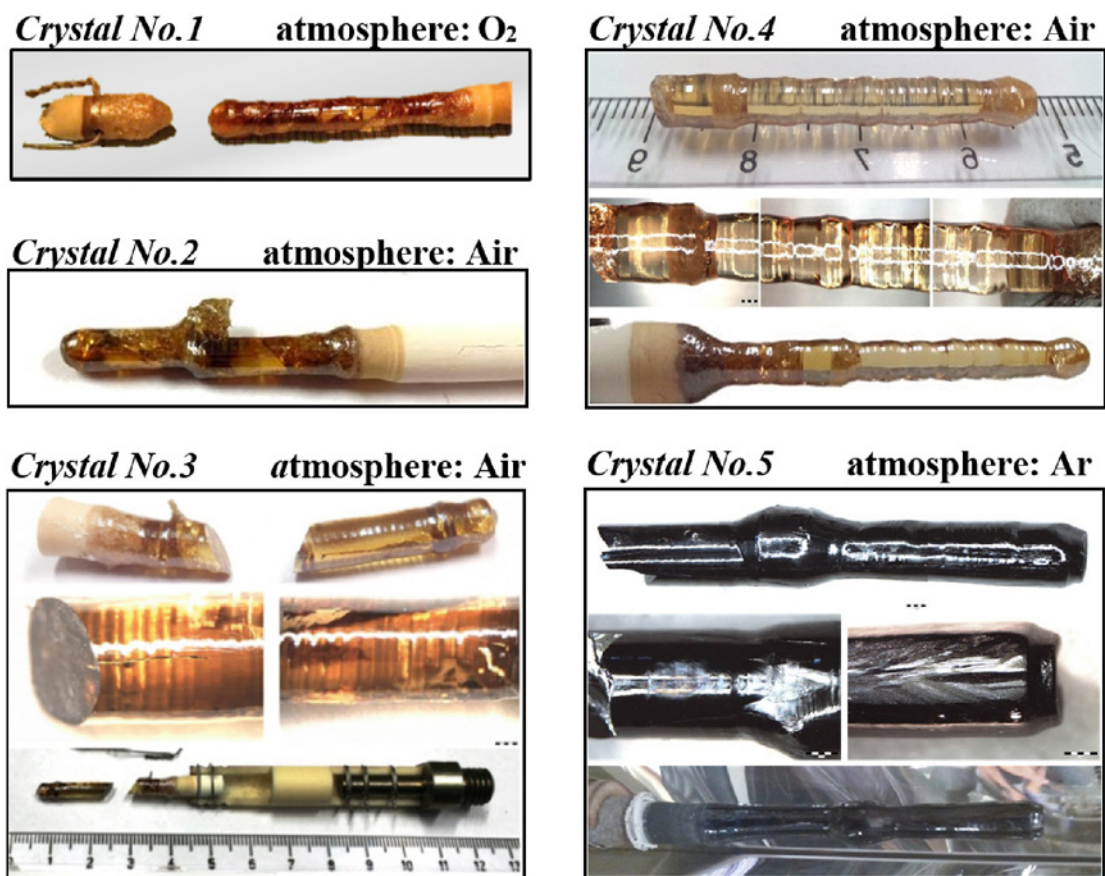


Fig. 4. Photos of the LaTiO_x grown single crystals – crystal growth parameters are presented in Tab. 1.

Table 1. Summary of crystal growth parameters for grown $\text{LaTiO}_{3+\delta}$ crystals

Crystal	Crystal growth conditions				Size diameter/length (mm)
	Growth rate (mm h^{-1})	Rotation rate (rpm)	Atm.	Lamp power	
No. 1	5	15	O_2	63.9–65.8	4/30
No. 2	6	15	Air	64–64.8	4/30
No. 3	8	15	Air	63.5–67.5 (70.3)	4/35
No. 4	5	15	Air	64.5–65.8	4/45
No. 5	6	15	Ar	63–64.5	4/40

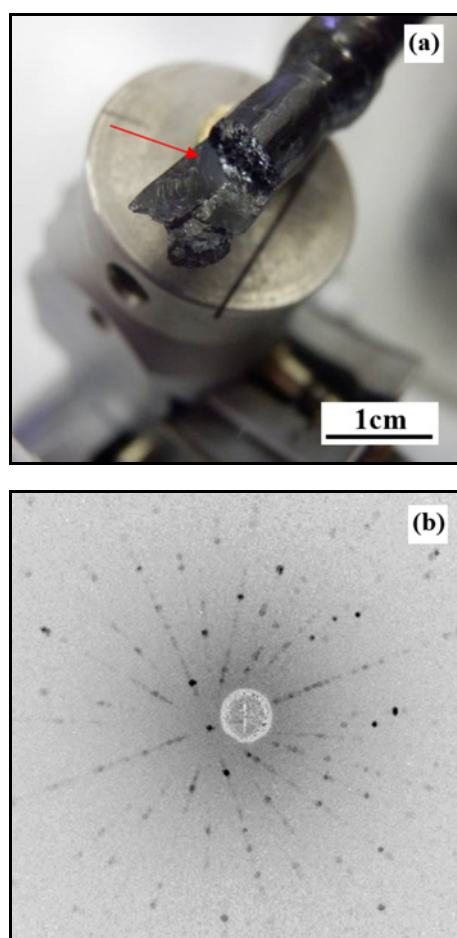


Fig. 5. The photos show (a) part of LaTiO_x crystal No. 5, which was grown in Ar atmosphere, placed on a goniometer – the red arrow points to the easy cleave plane = the boundary between two single crystals; (b) the corresponding Laue pattern.

quency induction heating [31, 32]. The referred optimal growing condition is a relatively small growth rate of $2\text{--}8\text{ mm h}^{-1}$ with counter-rotation of both feed and seed rod at $20\text{--}30\text{ rpm}$ in small overpressure of gas flow from 0.1 to 0.4 MPa [28–30]. The effect of crystal growth and annealing the crystals in different atmospheres (O_2 , Ar + O_2 , and Ar in gas flow) was studied and found to be very important [28–32]. The

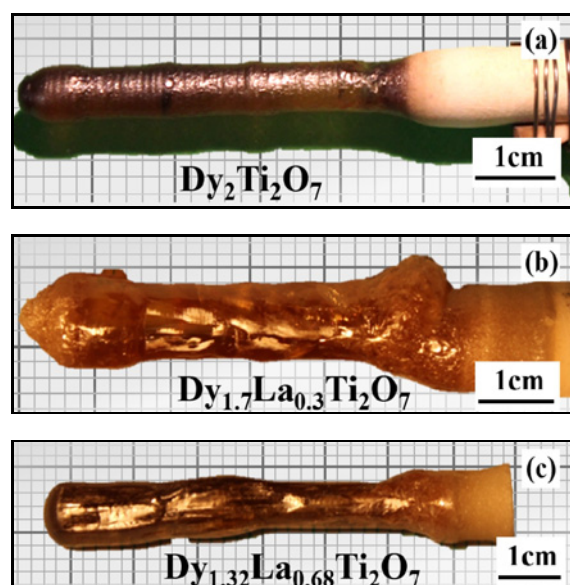


Fig. 6. Examples of single-phase $(\text{La}_{1-x}\text{Dy}_x)_2\text{Ti}_2\text{O}_7$ crystals.

amount of oxygen in the crystal affects the colour from black and opaque to dark amber semi-transparent and light yellow very well transparent [29]. In our case $(\text{Dy}_x\text{La}_{1-x})_2\text{Ti}_2\text{O}_7$ crystals where $x = 0.00, 0.15, 0.32, 0.50, 0.68, 0.85, 1.00$ were grown from starting materials La_2O_3 , Dy_2O_3 , and TiO under the flow of O_2 with small overpressure of about 0.1 MPa using the pulling rate of 5 mm h^{-1} with counter-rotation of both shafts 15 rpm . The seed rods and feed rods were prepared by sintering in the air at 1100°C . The examples of typical $(\text{Dy}_x\text{La}_{1-x})_2\text{Ti}_2\text{O}_7$ crystals are shown in Fig. 6. We prepared the crystals from 30 to 40 mm long with a diameter between 3 and 5 mm with a very regular shape (Fig. 6a). Most of the crystals developed facets (Figs. 6b,c) as they grew, and all of them were transparent to light with amber colour.

4. Crystal structure

XRPD measurements performed on powdered samples revealed that all LaTiO_x samples are sin-

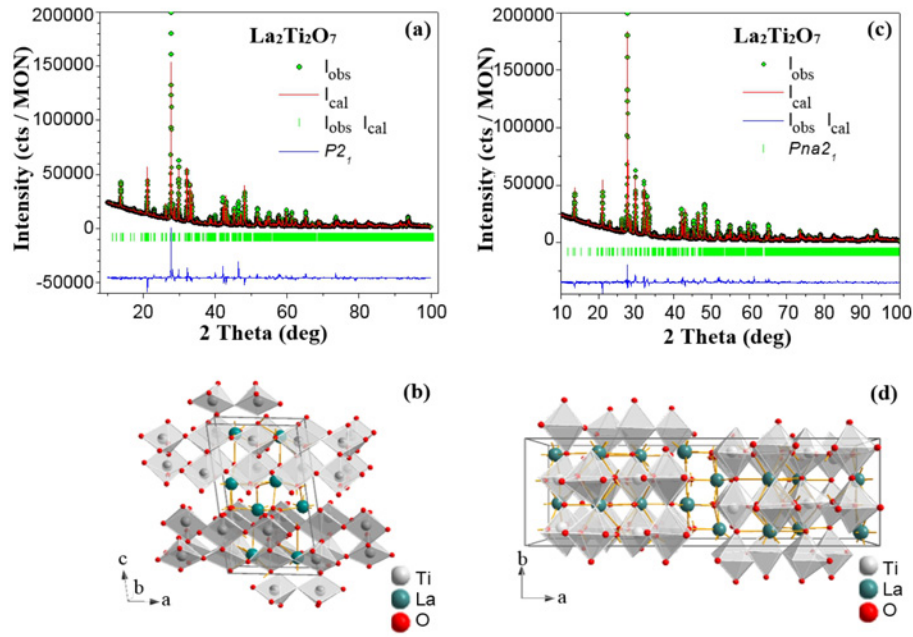


Fig. 7. Possible crystal structure of LaTiO_x crystal grown in O_2 ; (a) XRPD pattern, which was analysed by monoclinic model of the crystal structure space group $P2_1$, (b) the model of monoclinic structure made by program Diamond 3.0, (c) the XRPD pattern analysed by orthorhombic model of the crystal structure space group $Pna2_1$, (d) the model of orthorhombic structure.

Table 2. The crystal structure of $\text{LaTiO}_{3+\delta}$ crystals grown in the different atmosphere was determined within two possible crystal structure models. The more probable crystal structure is marked by bold characters

atmosphere	structure	a (Å)	b (Å)	c (Å)	V (Å ³)	β
air	$P121_1$	7.8246	5.5451	13.0215	558.4581	98.716°
air	$Pna2_1$	25.7399	7.8118	5.5488	1115.745	90.00°
O_2	$P121_1$	7.8130	5.5490	13.0205	558.1021	98.633
O_2	$Pna2_1$	25.7462	7.8126	5.5498	1116.3142	90.00°
Ar	$P121_1$	7.8118	5.5491	13.0182	557.9282	98.629
Ar	$Pna2_1$	25.7423	7.8121	5.5487	1115.976	90.00°

gle phase with no observed differences between the start and the end of any crystal. The analysis of the XRPD data leads to two possible structures, monoclinic $P2_1$ and orthorhombic $Pna2_1$, as it is demonstrated in Fig. 7 for $\text{LaTiO}_{3.5} = \text{La}_2\text{Ti}_2\text{O}_7$ grown in O_2 , where the same XRPD data were analysed by two different models $P2_1$ (Fig. 7a) and $Pna2_1$ (Fig. 7c) and the relevant crystal structures are presented in Figs. 7b,d. Polyhedrons with Ti atoms in the central position and oxygen atoms in vertices are basic building blocks of the crystal structure in both cases. Tetrahedrons are typical for $P2_1$ (Fig. 7b) and octahedrons, which are typical for 3D orthorhombic distorted perovskite structure, for $Pna2_1$ (Fig. 7d). Both crystal structures are members of the perovskite-related n -layered crystal structures $A_nB_nO_{3n+2}$ (n is a number of layers) [2]. $\text{La}_2\text{Ti}_2\text{O}_7$ ($\text{La}_4\text{Ti}_4\text{O}_{14}$) crystal structure is 4-type layered with typical slabs that are per-

pendicular to the longest crystal axis (c -axis or a -axis). An easy cleaved plane is perpendicular to the longest axis of the crystal lattice and is the consequence of the layered structure (see Fig. 4, crystal No. 3). The comparison of $I_{\text{obs}} - I_{\text{cal}}$ from Fig. 7a and Fig. 7c indicates that $Pna2_1$ model of crystal structure fits better with our experimental data. The characteristic crystal parameters for LaTiO_x crystals are summarised in Tab. 2 and Tab. 3. The $Pna2_1$ orthorhombic model of crystal structure describes a better crystal structure of crystals prepared in air and O_2 ; on the other hand, the monoclinic $P2_1$ crystal structure suits better for crystals prepared in Ar. The monoclinic $P2_1$ structure was approved in a larger number of papers [11–14] than the $Pna2_1$ orthorhombic crystal structure [15]. Our results indicate that the boundary between these two-layered crystal structures is narrow. The expected crystal structure of crystals prepared from La_2O_3 and

Table 3. Quality of determining crystal structure was tested within conventional Rietveld parameters R_p , R_{wp} , R_e , Chi_2 , Bragg R -factor R_{Bragg} and R_f -factor. The more probable crystal structure is marked by bold characters

atmosphere	structure	R_p	R_{wp}	R_e	Chi_2	R_{Bragg}	R_f
air	$P121_1$	59.0	59.7	8.67	47.51	52.1	35.1
air	$Pna2_1$	38.3	39.2	8.85	19.66	29.1	21.3
O ₂	$P121_1$	28.3	28.7	2.82	103.9	25.2	21.4
O₂	$Pna2_1$	24.8	22.9	2.97	59.61	20	19.9
Ar	$P121_1$	40.6	38.9	13.8	7.979	30.9	15.9
Ar	$Pna2_1$	45.6	52.6	13.9	14.27	35.2	18.0

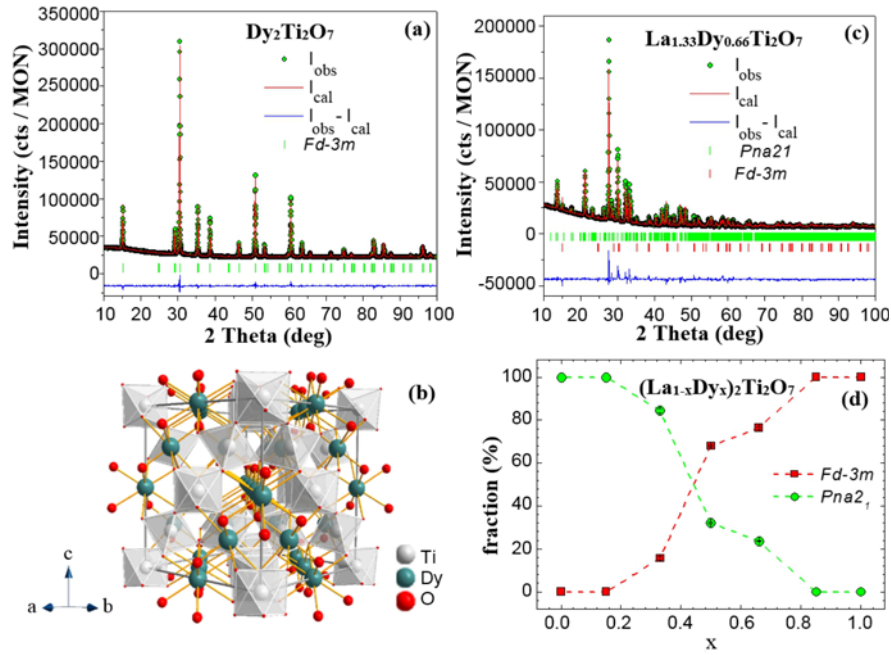


Fig. 8. Crystal structure of $(La_{1-x}Dy_x)_2Ti_2O_7$; (a) XRPD pattern of $Dy_2Ti_2O_7$ – cubic structure space group $Fd-3m$, (b) model of the cubic, (c) the XRPD pattern of $La_{1.33}Dy_{0.66}Ti_2O_7$ – cubic structure space group $Fd-3m$ and orthorhombic crystal structure space group $Pna2_1$, and (d) the effect of Dy substitution with La.

Ti_2O_3 starting materials in the Ar atmosphere was orthorhombic $Pbnm$ with chemical composition $LaTiO_3$. Our study based on XRPD measurements revealed that the crystal structure is monoclinic $P2_1$ and despite the fact that the colour of the crystals is the same as for $LaTiO_{3+\delta}$ [26], our results suggest higher oxygen content. In order to verify this suggestion, we performed the study of magnetic properties which is part of this paper.

XRPD measurements of powdered samples $(Dy_xLa_{1-x})_2Ti_2O_7$ confirmed the expected crystal structure of parent compounds $La_2Ti_2O_7$ and $Dy_2Ti_2O_7$ (Fig. 8a). The model of the pyrochlore crystal structure $Fd\bar{3}m$ of $(Dy_xLa_{1-x})_2Ti_2O_7$ is shown in Fig. 8b with TiO_6 octahedrons. Our results indicate that the solubility of dopant (La or Dy) in the parent compound is limited, two phases with different crystal structure $Pna2_1$ and $Fd\bar{3}m$ coexist in the range between $x = 0.32$ and 0.68 (Figs. 8c,d) and only sam-

ples for $x = 0.00, 0.15, 0.85, 1$ are single-phase materials (Fig. 8d). The longest a -axis of the orthorhombic structure is intact by substitution of La^{3+} by Dy^{3+} and both b - and c -axes decrease with substitution indicating the dominant effect on slabs of the layered structure. Lattice parameter of the cubic structure increases with substitution of Dy^{3+} ion by La^{3+} ion with larger ionic radius from 10.149\AA to 10.148\AA , 10.166\AA , 10.166\AA , 10.181\AA for $x = 1.00, 0.85, 0.68, 0.5,$ and 0.32 (Fig. 9d).

5. Magnetic properties

The temperature dependence of magnetisation (Fig. 10a) and hysteresis loop (Fig. 10b) indicate that $La_2Ti_2O_7$ is diamagnetic material which may contain traces of magnetic impurities with magnetic phase transitions at 56 and 10 K of ferrimagnetic ordering

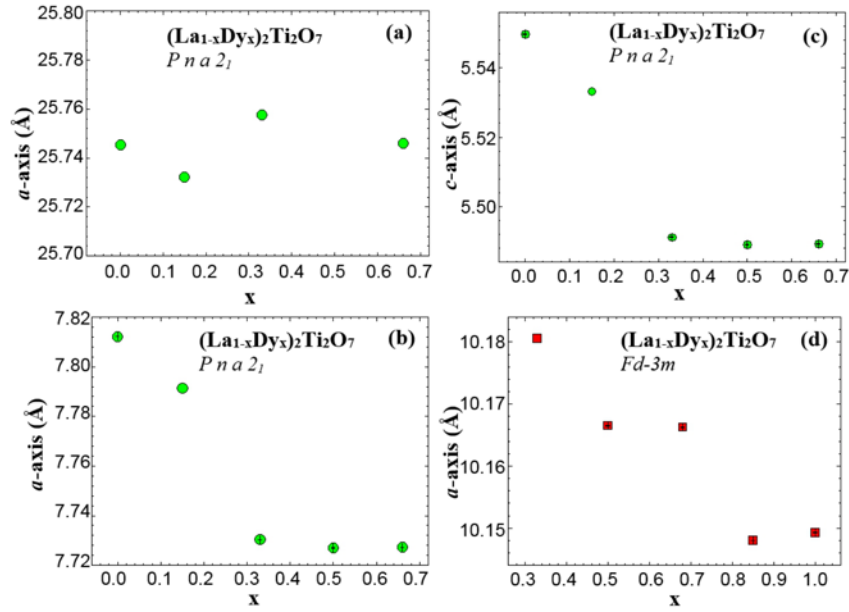


Fig. 9. Substitution effect on crystal lattice parameters of $(La_{1-x}Dy_x)_2Ti_2O_7$: (a) a -axis for the orthorhombic structure; (b) b -axis for the orthorhombic structure; (c) c -axis for the orthorhombic structure; and (d) a -axis for the cubic structure.

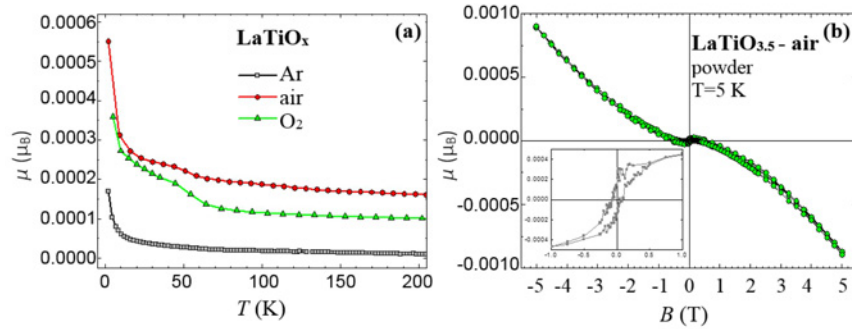


Fig. 10. Dependence of magnetisation for $LaTiO_x$ on (a) temperature for a different atmosphere and (b) magnetic field.

corresponding to small upturns in $\mu(T)$ (Fig. 10a). These impurities are not identical with Mott insulator $LaTiO_3$ with the Néel temperature $T_N = 146$ K [5]. Another conclusion can be made from the hysteresis loop shown in the inset of Fig. 10b, which provides evidence that weak ferromagnetic ordering is natural for $La_2Ti_2O_7$. Recently room temperature magnetisation measurements revealed ferromagnetic and ferroelectric behaviour for transition metals doped $La_2Ti_2O_7$ including the parent compound, too [34, 35], which proposes multiferroic character of this system. Our results correspond with already published magnetisation measurements, and the comparison of the curvature and the shape of magnetisation dependence $\mu(T)$ obtained on the sample with oxygen content $x = 3.41$ [2] with our measurements points to the fact that the content of oxygen in the crystal prepared in Ar atmosphere is even higher than $x = 3.41$ and supports our XRPD measurements which despite the dark colour of the crystals

revealed different crystal structure than $LaTiO_3$ crystal has.

The typical $\mu(T)$ dependences of $(Dy_xLa_{1-x})_2Ti_2O_7$ do not show any signs of magnetic phase transition (Fig. 11a). Three temperature ranges with different slope of $1/\chi(T)$ is the characteristic feature for the inverse susceptibility of $Dy_2Ti_2O_7$: high-temperature range from 360 to 200 K yielding the Curie Weis temperature $\theta = -44.4$ K, range from 190 to 40 K with $\theta = -7.7$ K and finally from 20 to 2 K with $\theta \approx 0.5$ K indicating reduction of antiferromagnetic correlations and evolution of small ferromagnetic correlations which have been already observed in vicinity of transition to ‘spin ice’ ground state at T_i [16]. Two of these ranges are shown in Fig. 11b. The change of the slope corresponds very well with the next highest excited state, which is expected to be around 200 K (Fig. 11a). Substitution of Dy^{3+} with nonmagnetic La^{3+} reduces the transition between high and low temperature regions from 150 to 50 K and antiferromagnetic correlation

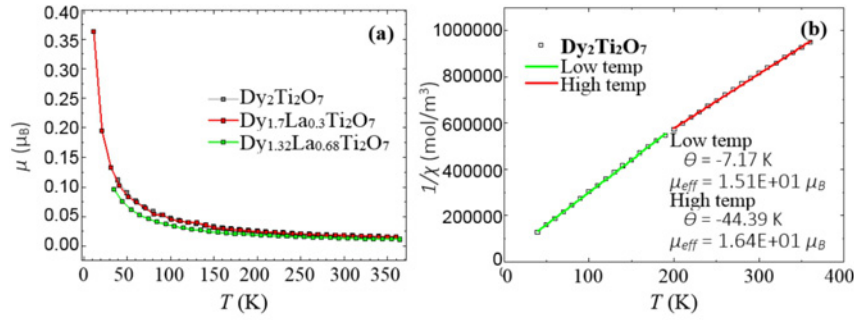


Fig. 11. Dependence of magnetisation for $\text{La}_{1-x}\text{Dy}_x\text{Ti}_2\text{O}_7$ on (a) temperature for a different atmosphere and (b) magnetic field.

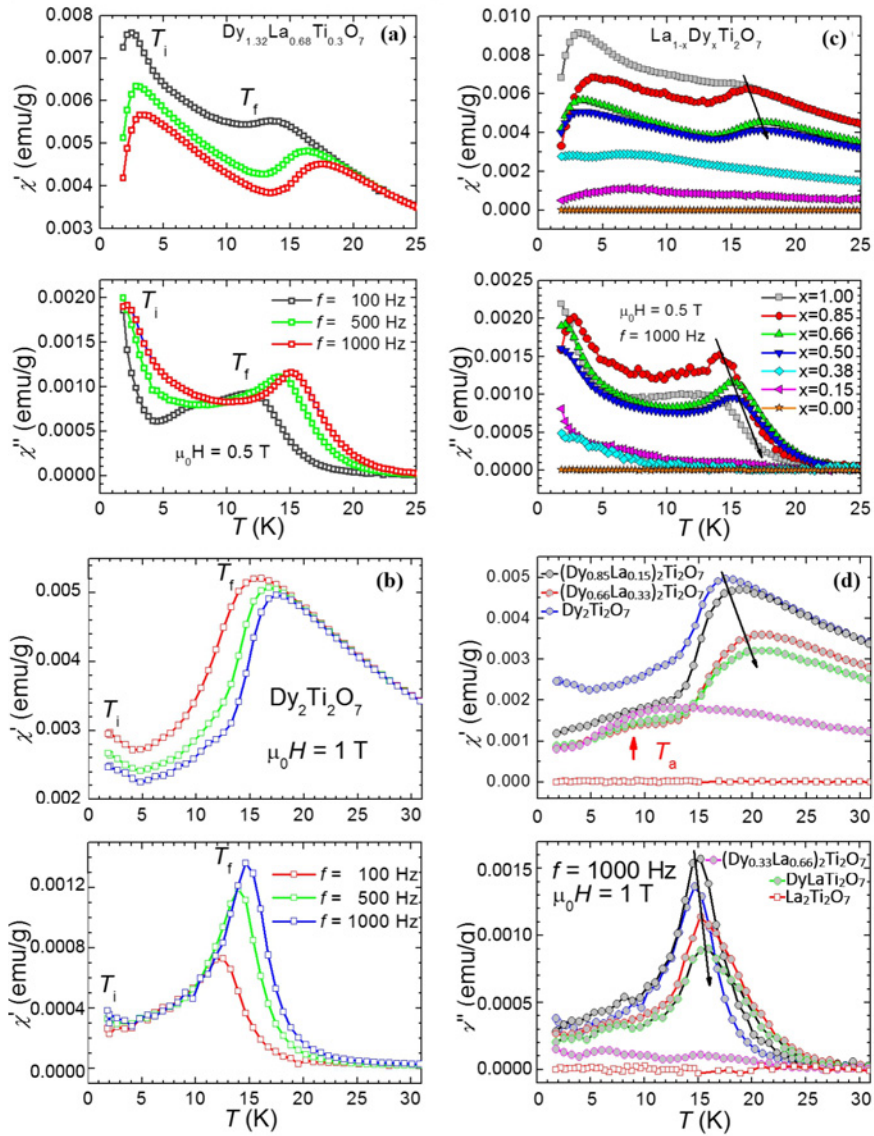


Fig. 12. Temperature dependence of AC susceptibility (both components in phase χ' and out of phase χ'' for $\text{La}_{1-x}\text{Dy}_x\text{Ti}_2\text{O}_7$) is displayed as a function of frequency f ; (a) $\text{Dy}_2\text{Ti}_2\text{O}_7$ in DC magnetic field 1 T, (b) $\text{Dy}_{1.32}\text{La}_{0.68}\text{Ti}_2\text{O}_7$ in DC magnetic field 0.5 T, (c) effect of substitution: x -content for magnetic field 1 T, and (d) effect of x -content for field 0.5 T.

from $\theta = -40.8$ K to $\theta = -7.3$ K for x from 0.85 to 0.32, respectively. The small ferromagnetic correla-

tions for the sample with $x = 0.85$ are suppressed and $\theta \approx 0.2$ K.

Two distinct strongly frequency and magnetic field dependent maxima, which are present in both in-phase component χ' and out-of-phase component χ'' of AC susceptibility, are a characteristic feature of $\text{Dy}_2\text{Ti}_2\text{O}_7$ (Figs. 12a,b). Their different frequency dependences suggest the existence of two different types of dynamical behaviour. One of T_i , observed below 2 K, is related to a highly degenerated ground state – ‘spin ice’ state and another to spin freezing at higher temperatures below $T_f \approx 10$ K [17–19]. The dynamical freezing behaviour seen in $\text{Dy}_2\text{Ti}_2\text{O}_7$ differs from the critical slowing down observed in conventional disordered spin-glass materials. In spin glasses, T_f decreases with increasing magnetic field strength, while in $\text{Dy}_2\text{Ti}_2\text{O}_7$, the opposite tendency is seen for applied magnetic fields. Our results of AC susceptibility measurements with respect to an applied DC magnetic field, frequencies of driving field and chemical composition, which are summarised in Fig. 12, confirm these basic features. The effect of the different magnetic field we demonstrate in Figs. 12a, 2b. Both maxima at T_i and T_f are very well visible in AC susceptibility for the magnetic field 0.5 T (Fig. 12a). The enlargement of the field to 1T shifts the maximum at T_f to a higher temperature and makes the maximum bigger (Fig. 12b). Our measurements indicate that strong frequency dependence of $\text{Dy}_2\text{Ti}_2\text{O}_7$ remains maintained on doped samples (Fig. 12a). Figures 12c,d summarise the effect of La substitution. The maximum at T_f shifts to higher temperature with La substitution (Figs. 12c,d) and a new anomaly at T_a marked by red arrow develops (Fig. 12d). The shift of T_f is evident, and the anomaly at T_a provides an indication of a new magnetic phase with $Pna2_1$ crystal structure or we see new dynamical behaviour in $Fd\bar{3}m$ phase below $x = 0.68$. Our AC results indicate enhanced dynamical behaviour which was already supposed for $\text{Dy}_2(\text{Ti}_x\text{Fe}_{1-x})_2\text{Ti}_2\text{O}_7$ material [33]. The reduction of the maxima in AC susceptibility can be attributed to the reduction of the cubic phase in the sample which may indicate that the feature known from the spin ice system is still strong and new dynamical behaviour develops. The T_i is not affected by substitution very much for the low concentration of dopant. The increase of the volume of the primary cell with La substitution is larger for a small concentration of dopant actually in the range of good solubility of La in $\text{Dy}_2\text{Ti}_2\text{O}_7$ and that is why the stronger effect on magnetic processes was observed for this concentration range.

6. Summary

In our paper, we focus on crystal growth and characterisation of $(\text{Dy}_x\text{La}_{1-x})_2\text{Ti}_2\text{O}_7$ crystals which were grown by optical floating zone technique in different

crystal growth conditions. The optimal pulling speed is about 6 mm per hour and counter-rotation of 15 rpm for both seed and feed rods for LaTiO_x crystals which were prepared in air, O_2 , or Ar atmosphere. In all cases, the final composition is close to $\text{LaTiO}_{3.5}$. The crystal structure varies between orthorhombic $Pna2_1$ (air, O_2) and monoclinic $P2_1$ (Ar). The colour of the crystals changes depending on the content of oxygen in the crystal from dark amber transparent colour for grown in O_2 , to light amber transparent colour for air and to almost opaque metallic shiny dark blue to black colour for Ar. Our study of LaTiO_x underlines the dominant effect of crystal growth conditions, especially gas surrounding the crystal structure, which may change the oxidation state of Ti even in the inert Ar atmosphere. Magnetic measurements confirmed properties which are expected for $\text{La}_2\text{Ti}_2\text{O}_7$ ferroelectric material and indicate very weak ferromagnetic properties for all samples. The study of $(\text{Dy}_x\text{La}_{1-x})_2\text{Ti}_2\text{O}_7$ system was the first one dealing with possible solubility of dopant in this type of parent compounds and was performed on crystals grown in O_2 atmosphere with pulling speed 5 mm per hour and counter-rotation of 15 rpm for both seed and feed rods. Prepared crystals were from 30 to 40 mm long with a diameter between 3 and 5 mm, sometimes with very regular shape. Most of the crystals developed facets as they grew, and all of them were transparent to light with amber colour. The solubility of dopant (La or Dy) in the parent compound is limited, two phases with different crystal structure $Pna2_1$ and $Fd\bar{3}m$ coexist in the range between $x = 0.32$ and 0.68 and only samples for $x = 0.00, 0.15, 0.85,$ and 1 are single phase. The longest a -axis of the orthorhombic structure is not intact by substitution of La by Dy and both b - and c -axes decrease with substitution. The lattice parameter of the cubic structure increases with the substitution of Dy^{3+} ion by La^{3+} ion with a larger ionic radius. The AC susceptibility measurements revealed that spin freezing temperature T_f shifts to higher temperature with La substitution and new anomaly at T_a marked develops providing evidence either of new magnetic phase with $Pna2_1$ crystal structure or creation of new dynamical behaviour of spins in $Fd\bar{3}m$ phase below $x = 0.68$ in the range between T_i and T_f . The transition to ‘spin ice’ ground state at T_i is not affected by substitution very much for the low concentration of La dopant. The frequency and magnetic field dependences of samples with pyrochlore structure resemble features typical for the $\text{Dy}_2\text{Ti}_2\text{O}_7$ spin frustrated system. The substitution of Dy by La opens a new possibility of tuning interesting magnetic properties of $\text{Dy}_2\text{Ti}_2\text{O}_7$ and can be used to study for a better understanding of multiferroic properties in this system.

Acknowledgements

This work was realized within the frame of the projects VEGA 2/0137/19 and “PROMATECH” ITMS: 26220220186.

References

- [1] F. Lichtenberg, D. Widmer, J. G. Bednorz, T. Williams, A. Reller, Phase diagram of LaTiO_x : from 2D layered ferroelectric insulator to 3D weak ferromagnetic semiconductor, *Zeitschrift für Physik B Condensed Matter* 82 (1991) 211–216. [doi:10.1007/BF01314010](https://doi.org/10.1007/BF01314010)
- [2] F. Lichtenberg, A. Herrnberger, K. Wiedenmann, J. Mannhart, Synthesis of perovskite-related layered $A_nB_nO_{3n+2} = ABO_x$ type niobates and titanates and study of their structural, electric and magnetic properties, *Progress in Solid State Chemistry* 29 (2001) 1–70. [doi:10.1016/S0079-6786\(01\)00002-4](https://doi.org/10.1016/S0079-6786(01)00002-4)
- [3] D. J. MacLean, H.-N. Ng, J. E. Greedan, Crystal structures and crystal chemistry of the $RE\text{TiO}_3$ perovskites: $RE = \text{La, Nd, Sm, Gd, Y}$, *Solid State Chem.* 30 (1979) 35–44. [doi:10.1016/0022-4596\(79\)90127-0](https://doi.org/10.1016/0022-4596(79)90127-0)
- [4] M. Eitel, J. E. J. Greedan, A high resolution neutron diffraction study of the perovskite LaTiO_3 , *Less Common Metals* 116 (1986) 95–104. [doi:10.1016/0022-5088\(86\)90220-1](https://doi.org/10.1016/0022-5088(86)90220-1)
- [5] M. Cwik, T. Lorenz, J. Baier, R. Müller, G. André, F. Bourée, F. Lichtenberg, A. Freimuth, R. Schmitz, E. Müller-Hartmann, M. Braden, Crystal and magnetic structure of LaTiO_3 : Evidence for nondegenerate t_{2g} orbitals, *Phys. Rev. B* 68 (2003) 060401(R). [doi:10.1103/PhysRevB.68.060401](https://doi.org/10.1103/PhysRevB.68.060401)
- [6] J. Goral, J. E. J. Greedan, The magnetic structures of LaTiO_3 and CeTiO_3 , *Mag. Mag. Mat.* 37 (1983) 315–321. [doi:10.1016/0304-8853\(83\)90062-8](https://doi.org/10.1016/0304-8853(83)90062-8)
- [7] G. Meijer, W. Heggeler, J. Brown, O.-S. Becker, J. Bednorz, C. Rossel, P. Wachter, Reduction of ordered moment in strongly correlated $\text{LaTiO}_{3+\delta}$ upon band filling, *Phys. Rev. B* 59 (1999) 11832–11836. [doi:10.1103/PhysRevB.59.11832](https://doi.org/10.1103/PhysRevB.59.11832)
- [8] T. Mizokawa, A. Fujimori, Electronic structure and orbital ordering in perovskite-type $3d$ transition-metal oxides studied by Hartree-Fock band-structure calculations, *Phys. Rev. B* 54 (1996) 5368–5380. [doi:10.1103/PhysRevB.54.5368](https://doi.org/10.1103/PhysRevB.54.5368)
- [9] B. Keimer, D. Casa, A. Ivanov, J. Lynn, M. von Zimmermann, J. Hill, D. Gibbs, Y. Taguchi, Y. Tokura, Spin dynamics and orbital state in LaTiO_3 , *Phys. Rev. Lett.* 85 (2000) 3946–3949. [doi:10.1103/PhysRevLett.85.3946](https://doi.org/10.1103/PhysRevLett.85.3946)
- [10] G. Khaliullin, S. Maekawa, Orbital liquid in three-dimensional Mott insulator: LaTiO_3 , *Phys. Rev. Lett.* 85 (2000) 3950–3953. [doi:10.1103/PhysRevLett.85.3950](https://doi.org/10.1103/PhysRevLett.85.3950)
- [11] S. Nanamatsu, M. Kimura, K. Doi, S. Matsushita, N. Yamada, A new ferroelectric: $\text{La}_2\text{Ti}_2\text{O}_7$, *Ferroelectrics* 8 (1974) 511–513. [doi:10.1080/00150197408234143](https://doi.org/10.1080/00150197408234143)
- [12] H. Yan, H. Ning, Y. Kan, P. Wang, M. J. Reece, Piezoelectric ceramics with super-high Curie points, *Am. Ceram. Soc.* 92 (2009) 2270–2275. [doi:10.1111/j.1551-2916.2009.03209.x](https://doi.org/10.1111/j.1551-2916.2009.03209.x)
- [13] Z. Gao, T. S. Suzuki, S. Grasso, Y. Sakka, M. J. Reece, Highly anisotropic single crystal-like $\text{La}_2\text{Ti}_2\text{O}_7$ ceramic produced by combined magnetic field alignment and templated grain growth, *J. Eur. Ceram. Soc.* 35 (2015) 1771–1776. [doi:10.1016/j.jeurceramsoc.2014.12.003](https://doi.org/10.1016/j.jeurceramsoc.2014.12.003)
- [14] F. X. Zhang, J. Lian, U. Becker, R. C. Ewing, L. M. Wang, J. Hu, S. K. Saxena, Structural change of layered perovskite $\text{La}_2\text{Ti}_2\text{O}_7$ at high pressures, *J. Sol. State Chem.* 180 (2007) 571–576. [doi:10.1016/j.jssc.2006.11.022](https://doi.org/10.1016/j.jssc.2006.11.022)
- [15] K. Scheunemann, Hk. Mueller-Buschbaum, Zur Kristallstruktur von $\text{Nd}_2\text{Ti}_2\text{O}_7$, *J. Inorg. Nucl. Chem.* 37 (1975) 2261–2263. [doi:10.1016/0022-1902\(75\)80723-8](https://doi.org/10.1016/0022-1902(75)80723-8)
- [16] A. Ramirez, A. Hayashi, R. J. Cava, R. Siddharthan, B. S. Shastry, Zero-point entropy in ‘spin ice’, *Nature* 399 (1999) 333–335. [doi:10.1038/20619](https://doi.org/10.1038/20619)
- [17] J. S. Gardner, M. J. P. Gingras, J. E. Greedan, Magnetic pyrochlore oxides, *Rev. Modern Phys.* 82 (2010) 53–107. [doi:10.1103/RevModPhys.82.53](https://doi.org/10.1103/RevModPhys.82.53)
- [18] K. Matsuhira, Y. Hinatsu, T. Sakakibara, Novel dynamical magnetic properties in the spin ice compound $\text{Dy}_2\text{Ti}_2\text{O}_7$, *J. Phys. Condens. Matter*, 13 (2001) L737–L746. [doi:10.1088/0953-8984/13/31/L01](https://doi.org/10.1088/0953-8984/13/31/L01)
- [19] J. Shi, Z. Tang, B. Zhu, P. Huang, D. Yin, C. Z. Li, Y. Wang, H. Wen, Dynamical magnetic properties of the spin ice crystal $\text{Dy}_2\text{Ti}_2\text{O}_7$, *J. Mag. Mat.* 310 (2007) 1322–1324. [doi:10.1016/j.jmmm.2006.10.846](https://doi.org/10.1016/j.jmmm.2006.10.846)
- [20] Z. Hiroi, K. Matsuhira, S. Takagi, T. Tayama, T. Sakakibara, Specific heat of Kagomé ice in the pyrochlore oxide $\text{Dy}_2\text{Ti}_2\text{O}_7$, *J. Phys. Soc. Japan* 72 (2003) 411–418. [doi:10.1143/JPSJ.72.411](https://doi.org/10.1143/JPSJ.72.411)
- [21] J. Lazúrová, M. Mihalik, M. Mihalik Jr., M. Vavra, M. Zentková, J. Briančin, M. Perovic, V. Kusigerski, O. Schneeweiss, P. Roupčová, K. V. Kamenev, M. Mišek, Z. Jagličić, Magnetic properties and Mössbauer spectroscopy of $\text{NdFe}_{1-x}\text{Mn}_x\text{O}_3$, *J. Phys. Conf. Ser.* 592 (2015) 012117. [doi:10.1088/1742-6596/592/1/012117](https://doi.org/10.1088/1742-6596/592/1/012117)
- [22] J. R. Carvajal, Recent advances in magnetic structure determination by neutron powder diffraction, *Physica B* 192 (1993) 55–69. [doi:10.1016/0921-4526\(93\)90108-I](https://doi.org/10.1016/0921-4526(93)90108-I)
- [23] S. M. Koohpayeh, D. Fort, J. S. Abell, The optical floating zone technique: A review of experimental procedures with special reference to oxides, *Progress in Cryst. Growth Char. Mat.* 54 (2008) 121–137. [doi:10.1016/j.pcrvsgrow.2008.06.001](https://doi.org/10.1016/j.pcrvsgrow.2008.06.001)
- [24] S. M. Koohpayeh, Crystal Growth of Functional Oxides Using Image Furnace. [Master Thesis] Birmingham, The University of Birmingham 2009.
- [25] M. Kestigian, R. Ward, The preparation of lanthanum titanium oxide, LaTiO_3 , *J. Am. Chem. Soc.* 76 (1954) 6027–6027. [doi:10.1021/ja01652a044](https://doi.org/10.1021/ja01652a044)
- [26] H. Roth, Single Crystal Growth and Electron Spectroscopy of d^1 -Systems, [PhD. Thesis] Cologne, University of Cologne 2008. (in German)
- [27] H. A. Dabkowska, A. B. Dabkowski, R. Hermann, J. Priede, G. Gerbeth, Handbook of Crystal Growth. 8 – Floating Zone Growth of Oxides and Metallic Alloys. Oxford, Elsevier 2015. [doi:10.1016/B978-0-444-63303-3.00008-0](https://doi.org/10.1016/B978-0-444-63303-3.00008-0)
- [28] G. Balakrishnan, O. A. Petrenko, M. R. Lees, D. McK Paul, Single crystal growth of rare earth titanate py-

- rochlores, *J. Phys. Condens. Matter.* 10 (1998) L723–L725. [doi:10.1088/0953-8984/10/44/002](https://doi.org/10.1088/0953-8984/10/44/002)
- [29] D. Prabhakaran, A. T. Boothroyd, Crystal growth of spin-ice pyrochlores by the floating-zone method, *J. Cryst. Growth* 318 (2011) 1053–1056. [doi:10.1016/j.jcrysgro.2010.11.049](https://doi.org/10.1016/j.jcrysgro.2010.11.049)
- [30] Q. J. Li, L. M. Xu, C. Fan, F. B. Zhang, Y. Y. Lv, B. Ni, Z. Y. Zhao, X. F. Sun, Synthesis, growth, characterisation and crystal structure of zinc cadmium thiourea complex $Zn_{0.625}Cd_{1.375}(CS(NH_2)_2)_{9.4}(SO_4)$, *J. Cryst. Growth* 377 (2013) 96–100. [doi:10.1016/j.jcrysgro.2013.04.048](https://doi.org/10.1016/j.jcrysgro.2013.04.048)
- [31] J. Kang, Z. Fang, X. Chen, W. Liu, F. Guo, S. Wu, Y. Zhang, J. Chen, Effect of oxygen vacancy concentration on the absorption spectra of $Dy_2Ti_2O_7$ crystal, *J. Alloys and Comp.* 599 (2014) 170–174. [doi:10.1016/j.jallcom.2014.02.081](https://doi.org/10.1016/j.jallcom.2014.02.081)
- [32] J. Kang, M. Ruan, X. Chen, C. Liu, W. Liu, F. Guo, J. Chen, Growth and magneto-optical characteristic of $Dy_2Ti_2O_7$ crystal, *Opt. Mat.* 36 (2014) 1266–1269. [doi:10.1016/j.optmat.2014.03.013](https://doi.org/10.1016/j.optmat.2014.03.013)
- [33] H. Liu, Y. Zou, L. Ling, L. Zhang, W. Tong, C. Zhang, Y. Zhang, Frustrated magnetism and dynamical properties in pyrochlore-type magnet $Dy_2Ti_{2-x}Fe_xO_7$, *J. Mag. Mag. Mat.* 369 (2014) 107–113. [doi:10.1016/j.jmmm.2014.06.031](https://doi.org/10.1016/j.jmmm.2014.06.031)
- [34] L. Sun, J. Hu, F. Gao, X. Kong, H. Qin, M. Jiang, Room-temperature ferromagnetism and ferroelectricity of nanocrystalline $La_2Ti_2O_7$, *J. Alloys and Comp.* 502 (2010) 176–179. [doi:10.1016/j.jallcom.2010.04.137](https://doi.org/10.1016/j.jallcom.2010.04.137)
- [35] G. Gong, Y. Qiu, G. Zerihun, Y. Fang, Ch. Yin, Ch. Zhu, S. Huang, S. Yuan, Multiferroic properties in transition metals doped $La_2Ti_2O_7$ ceramics, *J. Alloys and Comp.* 611 (2014) 30–33. [doi:10.1016/j.jallcom.2014.05.039](https://doi.org/10.1016/j.jallcom.2014.05.039)